


ORIGINAL ARTICLE

Open Access



On Energy Assessment of Titanium Alloys Belt Grinding Involving Abrasive Wear Effects

Mingcong Li¹, Shudong Zhao¹, Heng Li¹, Yun Huang^{1,2}, Lai Zou^{1,2} and Wenxi Wang^{1,2*} 

Abstract

Improved energy utilisation, precision, and quality are critical in the current trend of low-carbon green manufacturing. In this study, three abrasive belts were prepared at various wear stages and characterised quantitatively. The effects of abrasive belt wear on the specific grinding energy partition were investigated by evaluating robotic belt grinding of titanium plates. A specific grinding energy model based on subdivided tangential forces of cutting and sliding was developed for investigating specific energy and energy utilisation coefficient E_{UC} . The surface morphology and Abbott–Firestone curves of the belts were introduced to analyse the experimental findings from the perspective of the micro cutting behaviour. The specific grinding energy increased with abrasive belt wear, especially when the belt was near the end of its life. Moreover, the belt wear could lead to a predominance change of sliding and chip formation energy. The highest E_{UC} was observed in the middle of the belt life because of its retained sharp cutting edge and uniform distribution of the grit protrusion height. This study provides guidance for balancing the energy consumption and energy utilization efficiency of belt grinding.

Keywords Belt grinding, Wear, Specific grinding energy, Microtopography

1 Introduction

Titanium alloys are widely used as core components in extreme environments because of their excellent physical and chemical properties [1]. Aero-engine blades exhibit a high fatigue life that is critical in spacecraft or plane safety [2]. Nevertheless, taking into account the challenging machining properties of this material, coupled with its complex surface and high-performance requirements, precision machining remains a challenge [3, 4]. Currently, abrasive belt grinding is widely used as the final processing step to obtain an excellent machined surface quality and consistent titanium alloy parts because of its flexibility and versatility [5]. Research is focused on aspects such as belt condition monitoring [6, 7], surface integrity [8,

9], and robot-assisted path planning [10, 11]. According to carbon peak and carbon neutralisation construction objectives, reduction of energy consumption is a critical topic of research in manufacturing [12, 13]. Furthermore, understanding of specific grinding energy in processing is one of the important branches.

The specific grinding energy serves as a valuable indicator for assessing energy consumption during the grinding process [14]. Material removal is achieved by the interaction between an abrasive surface and the workpiece. Three interactions, namely rubbing, ploughing, and cutting, between the grit and workpiece have been investigated [15]. Rubbing and ploughing are not energy-efficient practices, as they do not effectively remove material; instead, they primarily generate heat [16]. Malkin et al. [17] conducted on the relationships between material properties, grinding parameters, and specific grinding energy. Additionally, specific energy models were formulated based on their findings. [17]. Khelouki et al. [18] performed an analysis based on cutting forces and determined the sliding friction coefficient.

*Correspondence:

Wenxi Wang
wx.wang@cqu.edu.cn

¹ College of Mechanical and Vehicle Engineering, Chongqing University, Chongqing 400044, China

² State Key Laboratory of Mechanical Transmissions, Chongqing University, Chongqing 400044, China



© The Author(s) 2023. **Open Access** This article is licensed under a Creative Commons Attribution 4.0 International License, which permits use, sharing, adaptation, distribution and reproduction in any medium or format, as long as you give appropriate credit to the original author(s) and the source, provide a link to the Creative Commons licence, and indicate if changes were made. The images or other third party material in this article are included in the article's Creative Commons licence, unless indicated otherwise in a credit line to the material. If material is not included in the article's Creative Commons licence and your intended use is not permitted by statutory regulation or exceeds the permitted use, you will need to obtain permission directly from the copyright holder. To view a copy of this licence, visit <http://creativecommons.org/licenses/by/4.0/>.

Furthermore, they separated the macroscopic specific grinding energy during belt grinding into cutting and sliding specific energy and revealed that the cutting energy is dominant in belt finishing process and can reach 75% of the total specific energy. Zhu et al. [19] divided the total specific grinding energy in the abrasive belt grinding processes into sliding, ploughing, and cutting. Unlike in Ref. [18], the predominant component is the sliding-specific energy, which can account for up to 50% of the entire total specific energy [19]. Subsequent research revealed that the force involved in chip formation remains detached from the predetermined normal forces, consequently leading to a reduced efficiency of approximately 9% [20]. Conversely, in belt grinding without force control, this percentage varies within the range of 15 to 25% [21].

Refs. [18–20] focused on investigating the influence of machining parameters, such as preset normal forces, and work speed, on the specific grinding energy partition. However, the impact of abrasive belt wear was not taken into account, while this factor varies over time during the grinding process. Typically, the abrasive belt takes the form of a single-layer coated abrasive, and its wear and consumption tend to be more pronounced compared to that of abrasive wheels. When the material was removed, belt topography features, such as shape and protrusion height grits, gradually changed [21], which resulted in the transition in the material removal mechanism [5]. These effects become apparent when grinding and polishing of challenging-to-machine materials, such as titanium alloys [22].

This study investigated the effect of belt wear on shape and protrusion height of grits and its effect on the cutting mechanisms and specific grinding energy partition in belt grinding for reducing the energy consumption. Abrasive belts at various wear stages were prepared, and the belt characteristics were evaluated. Comparative grinding experiments were executed to reveal the characterisation of cutting mechanisms generated by the prepared abrasive belts grinding of titanium alloys. The differences in the surface characteristics of the abrasive belts and their effect on the specific grinding energy partition were discussed.

2 Experimental Procedures

2.1 Preparation and Evaluation of Wear Abrasive Belts

Before analysing the effect of wear on specific grinding energy partition, understanding the wear degree of the abrasive belts and conducting quantitative wear evaluation is critical. Generally, grits are sufficiently sharp and Material removal rate was considered to be larger in the beginning of the belt life. The grits did not wear considerably and the MRR remained steady in the middle of

Table 1 Parameters of the pre-experimental process

Parameters	Value
Feed speed V_w (mm/s)	8
Grinding speed V_s (m/s)	10
Normal force F_n (N)	8
Workpiece material	TC4, HRC 30
Grinding length (mm)	80

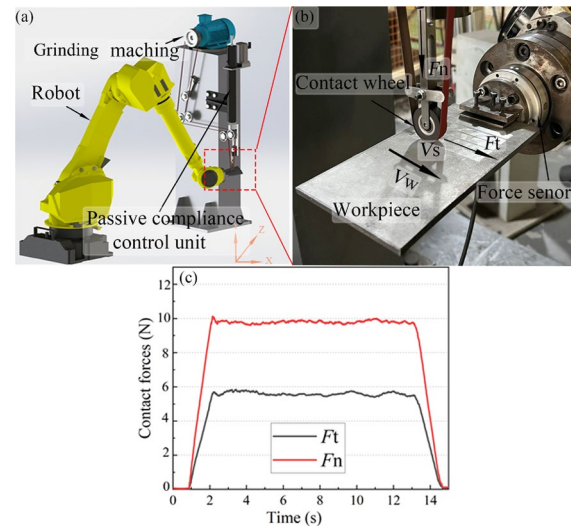


Figure 1 Experimental setup of robotic belt grinding: (a) Platform, (b) Grinding process, (c) Force profile with $V_s = 10$ m/s, $V_w = 5$ mm/s and $F_n = 10$ N using EOL-belt

the belt life. Finally, the grits wore severely and the MRR decreased considerably towards the end of life of the belt [23]. According to this pattern, typical abrasive belt wear behaviours include three periods, namely the initial, steady, and final periods [24].

Zirconium corundum abrasive belt P60, with particles measuring around $220 \mu\text{m}$, was employed. Based on a prior approach [25], three abrasive belts were prepared. The initial grinding with the abrasive belt was labelled as BOL-belt. After 50 rounds of grinding, it was referred to as MOL-belt. Lastly, the abrasive belt subjected to 130 rounds of grinding was termed EOL-belt. This investigation evaluated abrasive belt wear by assessing factors such as belt mass loss and material removal, as outlined in Table 1. The belt and workpiece weight were measured to obtain the mass loss by a precision electronic scale with a resolution of 0.001 g. Furthermore, the workpiece was ultrasonically cleaned with alcohol to ensure precise weight measurements.

All the grinding tests were performed on a robotic grinding platform displayed in Figure 1. The platform

incorporates an industrial robot, force sensor, and adaptive floating force control unit. The FANUC robot M-710iC/50 with improved positioning accuracy [26] was employed to execute the grinding trajectory. Force sensor KUNWEI R75B was mounted at the robot's end effector to measure the grinding force. The contact wheel, composed of cemented carbide as the core material and elastic rubber (H_s 50) as the outer layer, boasted a diameter of 30 mm and a width of 10 mm. TC4 plates,

sized at 200 mm × 100 mm × 10 mm, were chosen as the workpiece. The floating shaft was instrumental in real-time control of the stabilization of the normal grinding force. This control mechanism resulted in a remarkable 64.81% increase in the accuracy of normal grinding force control compared to the absence of such control measures [27]. Figure 1(c) displays a typical belt grinding force profile.

Material removal and belt loss decrease as the belt wear, as shown in Figure 2. This result was consistent with the abrasive belt grinding characteristics in typical belt wear periods. Furthermore, a digital microscope (VHX-1000C, Keyence) was used to evaluate the microscopic morphology of abrasive belts. The surface roughness and 2D local profile of belts were measured using a surface profiler (Intra Contour, Taylor Hobson), as shown in Figure 3. The belt surface becomes uniform as the belt wears and the fluctuation of the profile height becomes smaller. This result could also be proven by the decrease in the 2D roughness parameters, arithmetic mean deviation (R_a), and root mean square deviation (R_q) of the belts as the belt wear, which indicates a gradual decrease in the mean and variance of profile heights. These results are consistent with the basic law of abrasive belt wear.

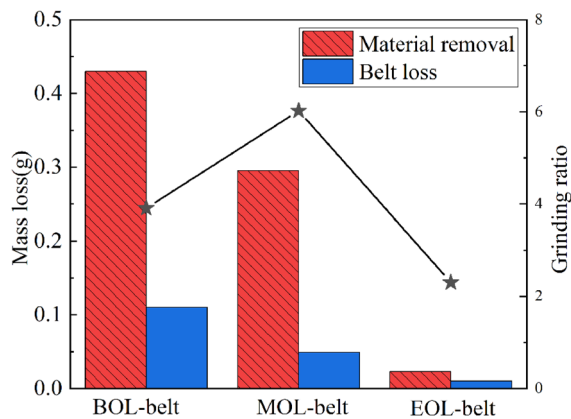


Figure 2 Grinding performance evaluation of belts

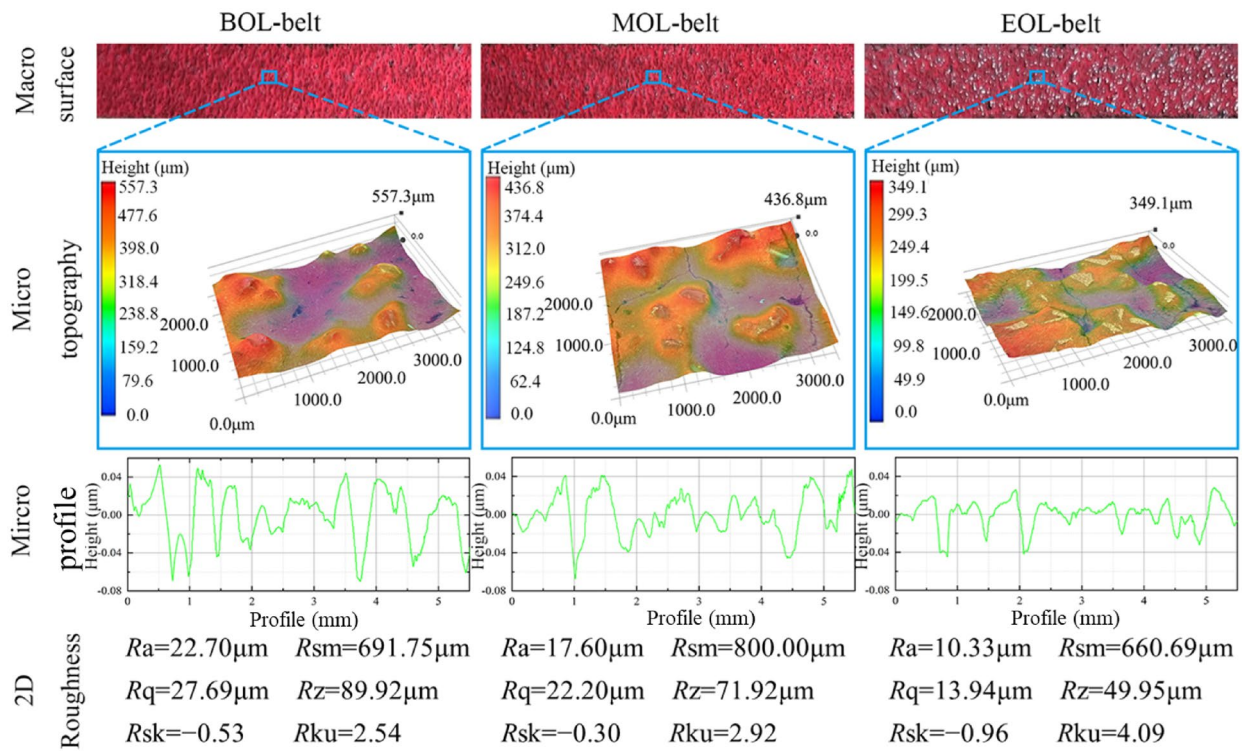


Figure 3 Macroscopic and microscopic of belts

Table 2 Parameters of the contrast experiment process

Parameters	Value
Feed speed V_f (mm/s)	5
Grinding speed V_s (m/s)	2, 3, 4, 6, 8, 10, 12
Normal force F_n (N)	10
Workpiece material	TC4, HRC 30
Grinding length (mm)	70
Contact wheel	$\Phi 30$ mm \times 10 mm

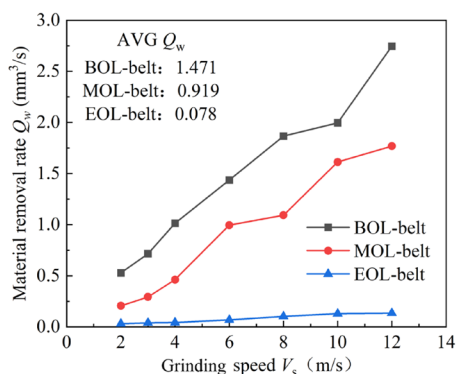


Figure 4 Material removal rate with various abrasive belts

2.2 Experimental Scheme

The grinding experiment was performed on the robotic grinding platform, as shown in Figure 1. A single-factor comparison experiment with 3 groups and 7 levels were conducted on TC4 plates (dimension of 100 mm \times 100 mm \times 10 mm) as depicted in Table 2. To remove the titanium plate after each test to measure the grinding ratio, the TC4 plate was levelled with a dual-axis angle protractor (DXL360S, Shanghai Grows Precision Instrument Co., Ltd.) before each grinding operation.

A single-point white-light confocal morphometry (PS50, Nanovea) with a noncontact measuring system was used to sample and analyse the surface morphology of the belts. A location along the length of the belt for measurement was randomly, the measurement area was 7 \times 21 mm², and the lateral sampling step was 10 μ m.

3 Experiment Results

3.1 Material Removal and Surface Roughness

Figure 4 shows the MRR in each of the 21 trials. The MRR increases with the increase of the grinding speed in all conditions, and the wear stage of the belt clearly corresponds to various MRR, with the average MRR

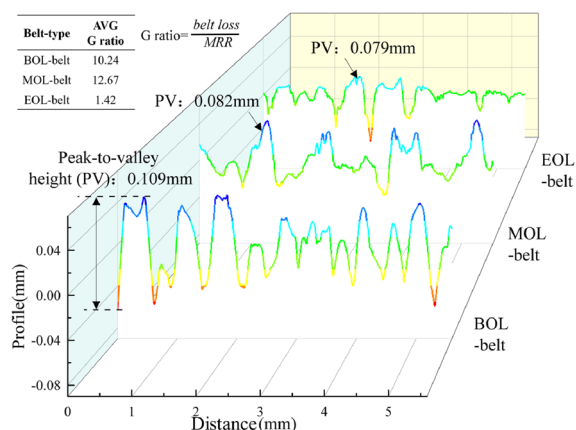


Figure 5 Micro profile of various abrasive belts

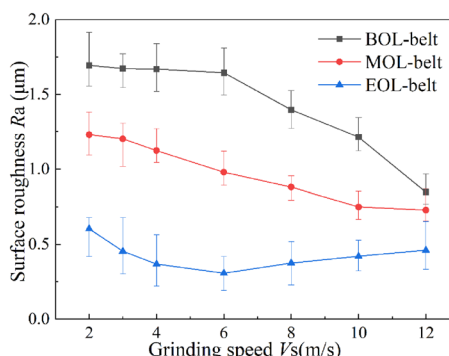


Figure 6 Surface roughness of TC4 ground for various abrasive belts

decreasing with the belt wear. The surface profile of BOL-belt exhibits uneven morphology, the highest peak-to-valley height (PV) value was 0.109 mm with a sharp feature, as shown in Figure 5. Grits that protrude prominently tend to possess robust penetration capabilities but are susceptible to fracturing due to elevated local pressures. Consequently, while the MRR is heightened, the grinding ratio remains comparatively low. For MOL-belt, the height of the peak and valley becomes more uniform with PV 0.082 mm, the grits penetration capability decrease as belt wear leads to low MRR. By contrast, the grits with lower tip protrusion and the self-sharpening edges are caused by fracture resulting in simultaneous grinding. Therefore, the grinding ratio was the highest. The MRR and grinding ratio of EOL-belt decreased severely as the plateaus dominated the surface features, and the wear flats grow remarkably, leading to an inability of the grit to cut the material.

Surface roughness of TC4 ground by various belts at different V_s are shown in Figure 6, and a decrease in average

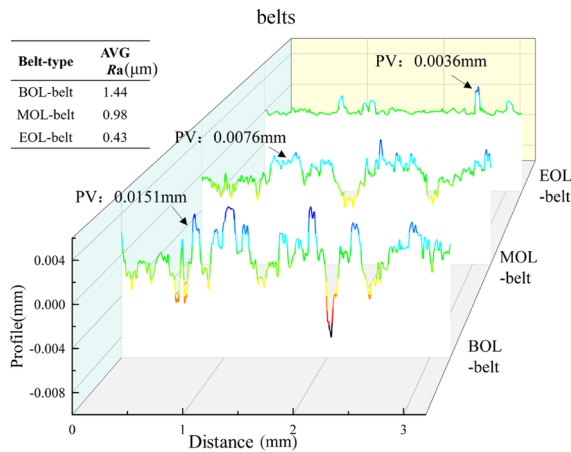


Figure 7 Micro profile of ground TC4 for various abrasive belts with $V_s = 6 \text{ m/s}$

R_a of the workpiece as belt wear can be observed from 1.44 to 0.98 μm and then to 0.43 μm . The average R_{sm} of the BOL-belt, MOL-belt, and EOL-belt were 175.70, 169.64, and 131.15 μm , respectively. Regarding the BOL-belt and MOL-belt, the surface roughnesses decreased with the increase of V_s speed. Furthermore, the uneven morphology of the belt was directly copied to the surface profile [28], as shown in Figure 7, which resulted in considerable unevenness of material removal on the surface ground by BOL-belt with the highest PV 0.0151 mm. Some sharp features also appeared at the TC4 ground of MOL-belt with PV reducing by 49% to 0.0076 mm, which indicated that the material was mainly removed by the uniform cutting edge. However, the local features were considerably reduced at the TC4 ground of EOL-belt with 0.00036 mm PV and the profile was the flattest.

3.2 Specific Grinding Energy and Energy Efficiency

The tangential forces (F_T) produced throughout the abrasive belt grinding process can be segregated into two distinct components: Cutting deformation force (F_C) and sliding force (F_S), which is similar to the wheel grinding forces. F_T can be expressed as follows:

$$F_T = F_C + F_S, \tag{1}$$

The overall force ratio (f) is defined as the proportion of tangential force to normal force (F_N) in the context of abrasive belt grinding:

$$f = \frac{F_T}{F_N} = \frac{F_C + F_S}{F_N}, \tag{2}$$

The sliding friction coefficient (μ_s) can be considered as follows:

$$\mu_s = \frac{F_S}{F_N}. \tag{3}$$

Eq. (3) can be rewritten as follows:

$$f = \mu_s + \frac{F_C}{F_N}, \tag{4}$$

Puthanangady and Malkin [29] focused on super finishing processes and adopted the assumption that the tangential cutting force is directly proportional to the removal rate Q_w . This relationship can be articulated as follows:

$$F_C = K \cdot Q_w, \tag{5}$$

where K is a constant, if applying this hypothesis to belt grinding, Eq. (5) can be rewritten as follows:

$$f = \mu_s + K \cdot \frac{Q_w}{F_N}. \tag{6}$$

In our preliminary pre-experiments, F_N was set as the experimental parameter, a line with an approximate level and negative slope was plotted from Eq. (6). This result was attributed to the fact that F_N is in some cases proportional to Q_w , which leads to the data points are clustered at a certain point of the ideal data, leading to incorrectly fitted curves. Therefore, V_s was selected as the experimental variable, the stability of F_N in each of 21 trials was ensured by using the force control unit for data accuracy (Figure 1).

The f versus Q_w / F_N curves are shown in Figure 8. The overall force ratio increases with the increase of Q_w in all conditions; this phenomenon is especially obvious in EOL-belt. The force ratio within abrasive machining serves as an indicator of the sharpness of the abrasive grits. the μ_s of BOL-belt, MOL-belt, and EOL-belt were 0.441, 0.374, and 0.427 μm , respectively.

Specific grinding energy (E_s) is defined as the ratio of machining power to the removal rate:

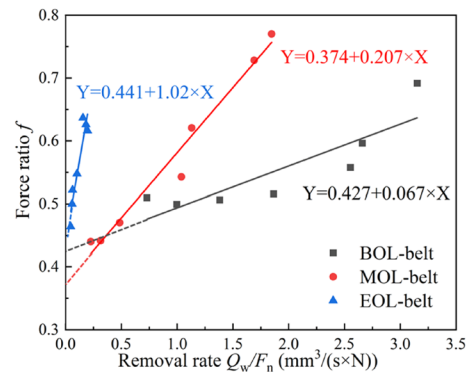


Figure 8 Overall force ratio versus material removal rate/normal force of various abrasive belts

$$E_s = \frac{V_C \cdot F_T}{Q_W} \tag{7}$$

The specific grinding energy (E_s) consists of cutting and sliding contributions E_{SC} and E_{SS} :

$$E_s = E_{SC} + E_{SS} \tag{8}$$

Each contribution can be expressed as follows:

$$E_{SC} = \frac{F_C \cdot V_C}{Q_W} \tag{9}$$

$$E_{SS} = \frac{F_S \cdot V_C}{Q_W} \tag{10}$$

By knowing μ_s , the specific cutting energy (E_{SC}) and specific sliding energy (E_{SS}) of the belts with various wear stages can be calculated, as shown in Figure 9. The E_s increases with the increase of V_s in all most conditions, and the average E_s of BOL-belt, MOL-belt, and EOL-belt were 1.807, 4.113, and 30.674 J/mm³. The high protrusion of grits of BOL-belt, combined with the sharp features, resulted in higher grits penetration and cutting ability of the BOL-belt with a large Q_W , which led to the lowest E_s . However, the highest E_s of the EOL-belt can be attributed to its lowest Q_W , the wear-flat grits require more energy to remove a unit volume of material.

From the perspective of material removal, only the specific cutting energy E_{SC} components in specific grinding energy (E_s) contribute directly to chip formation. Therefore, the ratio between the two can be defined as the energy utilisation coefficient (E_{UC}) in the grinding process as follows:

$$E_{UC} = \frac{E_{SC}}{E_s} \tag{11}$$

The removal rate was selected as the horizontal axis of the E_{UC} rather than the experimental variable grinding speed to be more relevant to engineering practice. By knowing the Q_W , the belt grinding E_{UC} is shown in Figure 10. E_{UC} increases with the increase of Q_W in all most conditions. In this study, higher Q_W was achieved by the increase of the grinding speed, which allowed more material to be removed per unit with effective grits. This result achieved a higher E_{UC} . From the perspective of energy efficiency, using the higher grinding speed is beneficial, but a small removal rate is effective in reducing the specific grinding energy (Figure 9). Moreover, MOL-belt exhibited the highest E_{UC} when Q_W is greater than 0.5 mm³/s. When the wear state of the abrasive belt reached the steady period, the grits with relative lower tip protrusion and the self-sharpening edges due to fracture initiate actual chip formation concurrently. This results in an augmentation of the count of effective cutting grits [24]. The homogeneous distribution of grits results in more grits participating in actual cutting, which results in higher grinding efficiency.

Comparing the various belts, the MOL-belt exhibited the highest energy efficiency, whereas the BOL-belt exhibited the lowest specific grinding energy. The range of fluctuations of E_s from 5% to 51% was considerably greater than the belt grinding experiments of TC4 with a ratio between 15% and 20% under the given conditions [19]. This result can be attributed to the distinct characteristics of the grits. The plausible mechanism of such phenomena caused by various micro cutting mechanisms in grinding is discussed in the subsequent section using 3D belt topography.

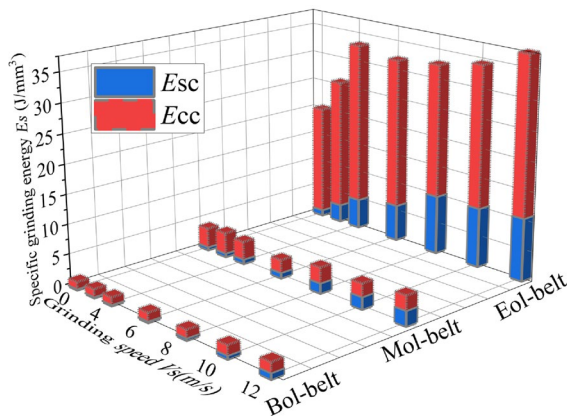


Figure 9 Specific grinding energy and its contributions versus the grinding speed

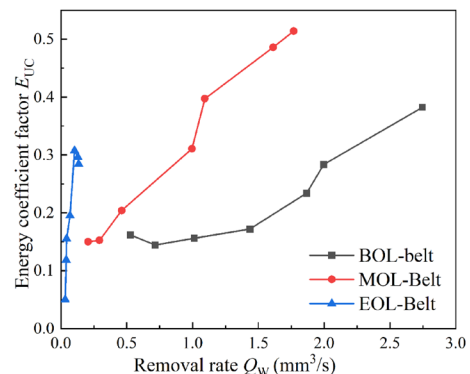


Figure 10 Energy utilisation coefficient versus the material removal rate

4 Discussions

4.1 Belt Surface Morphology

The shapes and distribution patterns of grits have a direct impact on micro cutting mechanisms and play a significant role in dictating the allocation of grinding energy. In abrasive belts, grits are electrostatically oriented to form sharp peaks to maximise cutting potential [30]. Thus, the sharp feature on the surface of the belt can be equated to the grits, and the summit features correspond to the state of the cutting edge, and the 3D profile of the abrasive

belt are shown in Figure 11. By analysing the profile data, number of grits in 7 mm × 21 mm and the probability of height distributions can be determined as shown in Figure 11(c). The height distribution of grits is segmented using the watershed lines transform [31]. The variation in peaky and plateaued type of surfaces illustrate the effect of belt wear on the condition of the grits. As mentioned, the BOL-belt exhibited sharp features, part of the grits with highest protrusion. Figure 11(e) shows that only most prominent grits are worn, and MOL-belt produced

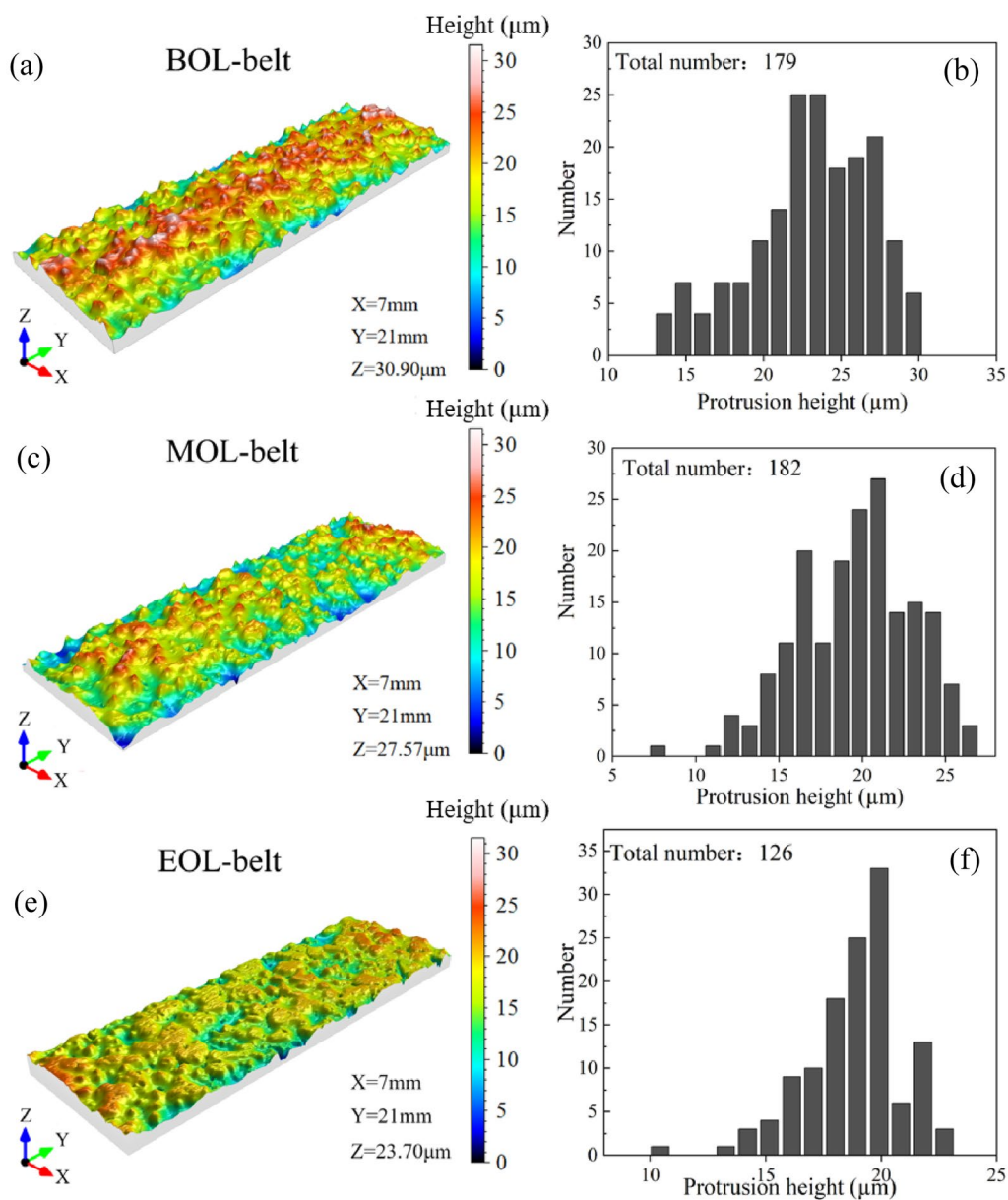


Figure 11 Distribution of grits: (a), (c), (e) 3D profile of belt topography, (b), (d), (f) Height distribution of grits

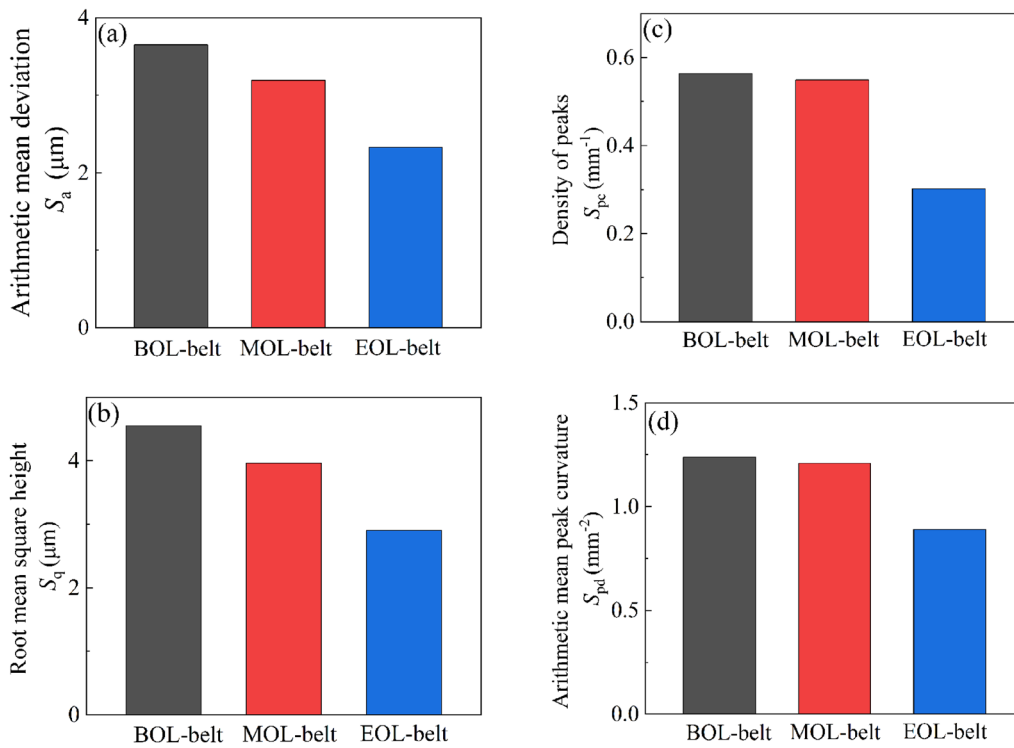


Figure 12 (a), (b) ISO 25178 height parameters, (c), (d) Feature parameters of abrasive belts

a homogeneous distribution of grits protrusion height. Because of the self-sharpening nature of ceramic grits, the wear renews the grits by creating new cutting edges and preserves the cutting ability. However, the wear-flat of most grits can be observed on EOL-belt, with the lowest number of grits as the interaction of cyclic stress of the belt. The cutting ability of the belt deteriorates, which lead to the lowest Q_w and highest E_s .

ISO 25178 height and feature parameters were applied to investigate the characteristics of the grits (Figure 12). A decrease in the overall height parameters as belt wear can be observed from 3.652 to 3.192 μm and then to 2.328 μm in the case of arithmetic mean deviation (S_a), and from 4.549 to 3.962 μm , and then to 2.902 μm in the case of root mean square height (S_q). Here, S_{pd} is the density of peaks, and S_{pc} is the arithmetic mean peak curvature. Regarding the uniform orientation of the grits, the feature parameters can be defined as describing the cutting edge characteristics of the grits. BOL-belt and MOL-belt exhibit similar feature parameters, which suggest a dense and sharp slope cutting edge distribution in the surface morphology. An apparent peak reduction and angularity variation can be identified for EOL-belt because of belt wear. With sharp summit angles of grits, the belt exhibits a greater ability to cut and remove material than the flat belt. By contrast, the heightened summit angle of the grits during belt grinding is conducive to promoting the sliding mechanism.

The grits are bonded onto the base of the belt as depicted in Figure 11(a). As shown in Figure 13, because of the various protrusion heights, the penetration depth of each grits differs. Thus, some grits, called inactive grits, do not touch the workpiece, and some grits, called active grits, contact and interact with the workpiece. Active grits are classified into two groups, namely sliding and cutting grits, according to the interaction between grits and workpiece. At the sliding stages, the deformation of the workpiece caused by the grits is fully elastic or elastic-plastic, and no material removal exists. At the cutting stage, the deformation is fully plastic and the material is removed. Therefore, the cutting grits are defined as effective grits.

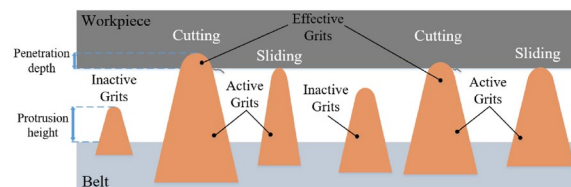


Figure 13 Schematic of the interaction between the belt and workpiece

4.2 Abbott–Firestone Curves of the Belt

The tribological potential of belt surface topography is characterised by the Abbott–firestone curves (AFC), serving as a representation of the scale-limited surface’s bearing ratio [32]. Furthermore, this approach enables the computation of a set of descriptors characterizing the material profile’s geometry. These descriptors encompass S_{pk} (the height of the peak portion), S_k (the height of the core portion), and S_{vk} (the depth of the valley portion) [33]. In Figure 14(b), the minimum-slope secant line spanning 40% of the AFC is illustrated. In accordance with ISO 25178 standards, the intersection with the curve delineates the boundaries between the aforementioned segments. Subsequently, horizontal segments extending from these points to the curve divide it into three distinct regions: Hill, core, and valley regions, and V_{MP} , V_{MC} , and V_{VC} reflect the material volume in the hill, core, and valley area, respectively. As shown in Figure 14(c), the surface profile of grits can be roughly categorised into three parts, namely hill, core, and valley areas, and the hill area of grits is most likely to penetrate into and remove material with grinding force. Thus, V_{MP} is considered to be the

contact area volume of effective grits, and V_{MC} and V_{VC} are the grit volume, which eventually exhibits running-in wear.

The AFC with statistical distribution of surface heights exhibits a Gaussian type profile of surface height distribution for the belts (Figure 15). The belt wear exhibits limited effect in valley area (material percentage > 90%) whereas in hill areas (material percentage < 10%), large diversity occurs, and the upper limit of the hill profile decreases with belt wear. These three belts exhibited a higher concentration of the surface in the core range (height ~17.5 μm), which results in a certain symmetry between peaks and valleys. Therefore, these results confirmed that an abrasive belt wear process may have occurred continuously in some severely damaged in hill area, which consequently removes the highest peaks while leaving the core and valleys less affected. Therefore, the hill area of the belt plays a dominant role in the interaction with the workpiece during the grinding process.

Figure 16(a) shows that the BOL-belt exhibits the highest sum of S_k , S_{pk} , and S_{vk} , which suggests a wider spread of grits protrusion height with a superior wear

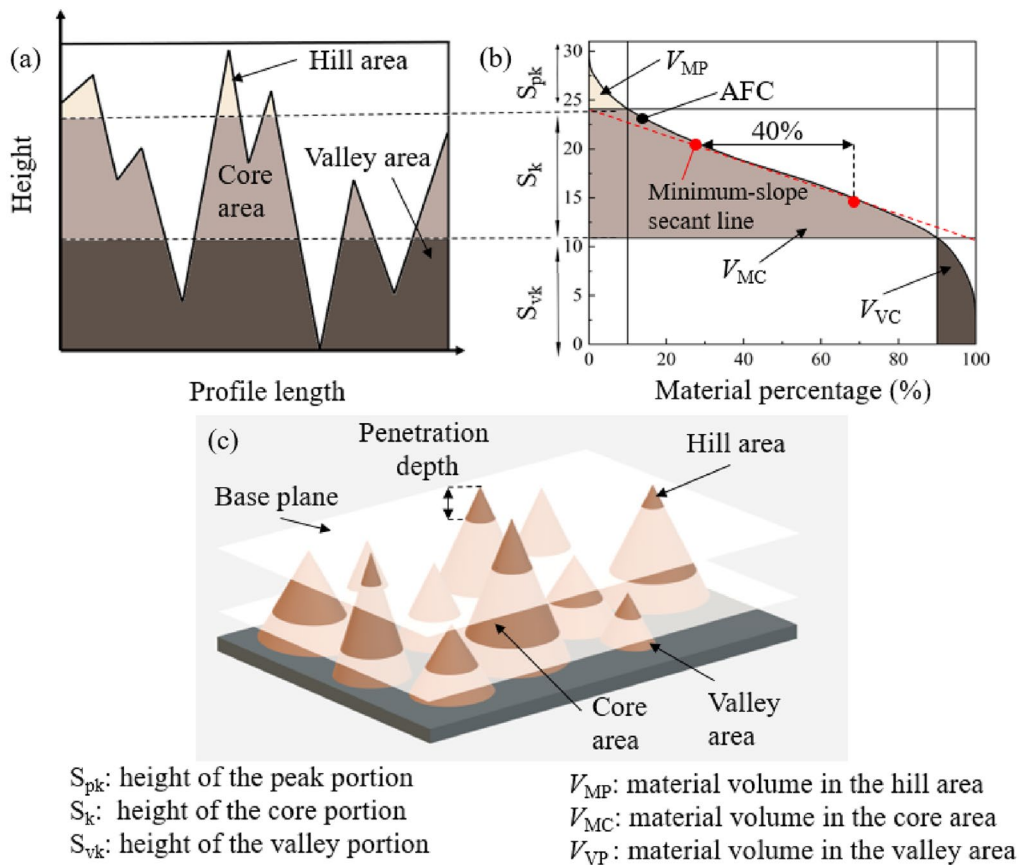


Figure 14 Schematic of the functional parameters: (a) Sketch of cross-section profile, (b) Functional parameters of AFC defined (ISO 25178), (c) Sketch of the belt profile

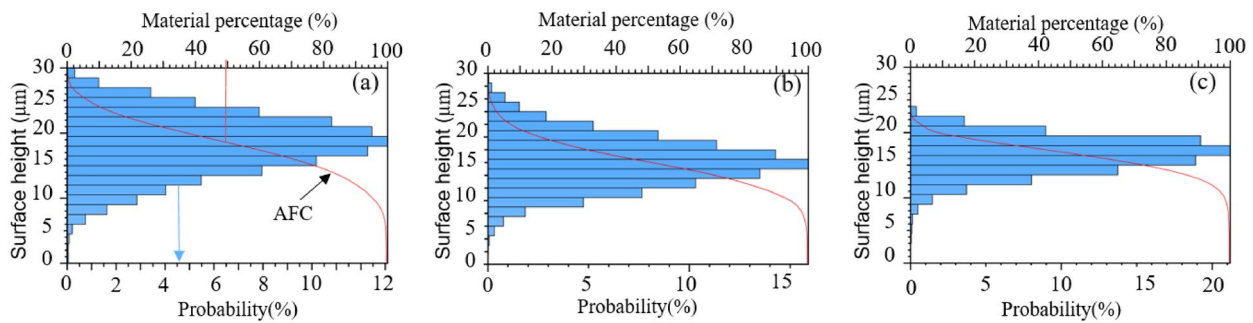


Figure 15 AFC of the belts: (a) BOL-belt, (b) MOL-belt, (c) EOL-belt

resistance compared with belts that exhibit wear. The high S_{pk} for the MOL-belt indicates the hill area of belt is composed of grits of similar protrusion height with tribological stability. EOL-belt rendered lowest S_{pk} , S_k and S_{vk} , which results in a small number of grits contact with the workpiece under the F_N with short service life. The material volume may be considered as an extension of the height measurement and provides insight into the interaction between the cutting edge of grits and

the material. Given that only a small proportion of the abrasive particles that reach a certain height can participate in the cutting, diverse V_{mp} can be obtained by changing the ratio of the material by moving the baseline plant as shown in Figure 16(a), and V_{mp90} is defined as the material volume when the reference plane is selected to a material ratio higher than 90%. MOL-belt exhibits the highest V_{mp} for various base planes, which causes considerable contact area between the grits and the workpiece, combined with the sharp feature of the grits (Figure 12) and high S_{pk} . This phenomenon suggests that more cutting mode occurs during the grinding process. With a uniformly distributed grits, the belt exhibits a higher cutting ability and material removal than the irregular grit. By contrast, the diverse distributed grits induce the sliding mechanism for grits with low protrusion height.

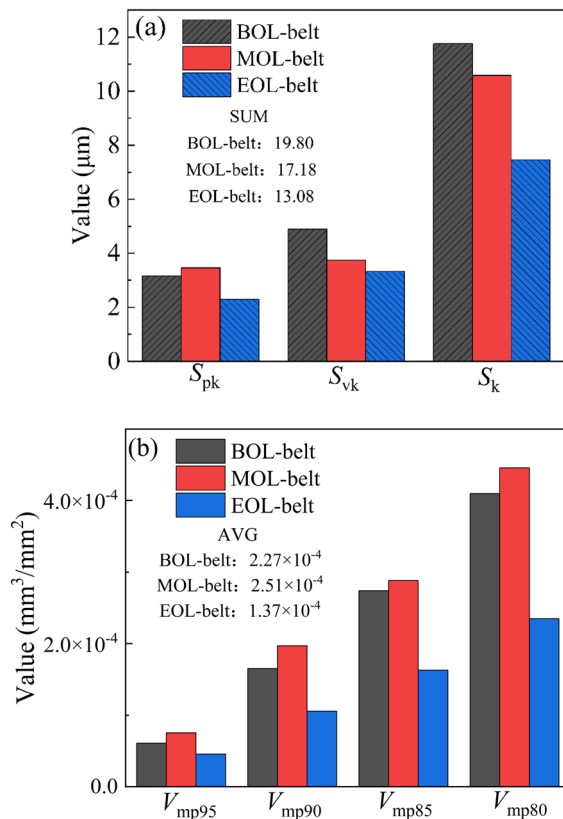


Figure 16 Functional parameters of AFC: (a) S_{pk} , S_k and S_{vk} , (b) V_{MP} with various material percentage

5 Conclusions

To investigate the effect of abrasive belt wear on the specific grinding energy in belt grinding, three belts at different wear stages were prepared. The effect of belt wear on the specific grinding energy of belt grinding titanium plate was investigated. The main conclusions can be summarised as follows.

- (1) It is experimentally found that abrasive belt wear can essentially cause an increase in grinding specific energy, because the initial grits with a high penetration depth will gradually be wear-flatted with lower protrusion height as the abrasive belt wears, leading to more energy consumption.
- (2) For each abrasive belt, E_{UC} increases with MRR and its slope rise with abrasive belt wear. Except in the low MRR phase, the moderate wear belt has higher E_{UC} than others, because its self-sharpening nature brings a more homogenization of the grits' shape and height, and more effective grits.

Acknowledgements

Not applicable.

Authors' Contributions

WW and YH contributed to the conception of the study; ML and SZ performed the experiment; ML and HL contributed to analysis and manuscript preparation; ML and SZ performed the data analyses and wrote the manuscript; WW and LZ helped perform the analysis with constructive discussions. All authors read and approved the final manuscript.

Authors' Information

Mingcong Li, born in 1996, is currently a PhD candidate at *College of Mechanical and Vehicle Engineering, Chongqing University, China*. His research interests include preparation and performance of compliant grinding tools.

Shudong Zhao born in 1996, is currently a master candidate at *College of Mechanical and Vehicle Engineering, Chongqing University, China*. His research interests include abrasive belt wear condition detection and life prediction.

Heng Li, born in 1999, is currently a PhD candidate at *College of Mechanical and Vehicle Engineering, Chongqing University, China*. His research interests include high performance manufacturing of aero blades.

Yun Huang, born in 1962, is currently an professor at *State Key Laboratory of Mechanical Transmissions, Chongqing University, China*. He received his PhD degree from *Chongqing University, China*. His research interests include advanced manufacturing technology and intelligent manufacturing and equipment.

Lai Zou, born in 1989, is currently an professor at *State Key Laboratory of Mechanical Transmissions, Chongqing University, China*. He received his PhD degree from *Harbin Institute of Technology, China*. His research interests include robotic intelligent processing technology and equipment.

Wenxi Wang, born in 1990, is currently an assistant researcher at *State Key Laboratory of Mechanical Transmissions, Chongqing University, China*. He received his PhD degree from *Beijing Jiaotong University, China*. His main research interests include grinding dynamics analysis and grinding surface quality control.

Funding

Supported by National Natural Science Foundation of China (Grant No. 52105430), China Postdoctoral Science Foundation (Grant No. 2020M673126), and Chongqing Municipal Natural Science Foundation of China (Grant No. cstc2020jcyj-msxmX0266).

Data availability

Data will be made available on request.

Declarations

Competing Interests

The authors declare no competing financial interests.

Received: 9 May 2022 Revised: 23 August 2023 Accepted: 1 September 2023

Published online: 12 October 2023

References

- [1] S Bratan, T Stadnik, V Golovin. Evaluation of effectiveness of cutting fluids for belt grinding of long-length products of titanium alloys. *Materials Today: Proceedings*, 2020, 38: 2013-2018.
- [2] Q Miao, W F Ding, J H Xu, et al. Creep feed grinding induced gradient microstructures in the superficial layer of turbine blade root of single crystal nickel-based superalloy. *International Journal of Extreme Manufacturing*, 2021, 3(4): 045102.
- [3] Y Cao, J F Yin, W F Ding, et al. Alumina abrasive wheel wear in ultrasonic vibration-assisted creep-feed grinding of Inconel 718 nickel-based superalloy. *Journal of Materials Processing Technology*, 2021, 297: 117241.
- [4] M W Gong, L Zou, H N Li, et al. Investigation on secondary self-sharpness performance of hollow-sphere abrasive grains in belt grinding of titanium alloy. *Journal of Manufacturing Processes*, 2020 59: 68-75.
- [5] D H Zhu, X Z Feng, X H Xu, et al. Robotic grinding of complex components: a step towards efficient and intelligent machining – challenges, solutions, and applications. *Robotics and Computer-Integrated Manufacturing*, 2020, 65: 101908.
- [6] W Caesarendra, T Triwiyanto, V Pandiyan, et al. A CNN prediction method for belt grinding tool wear in a polishing process utilizing 3-axes force and vibration data. *Electronics*, 2021, 10(12): 1429.
- [7] V Pandiyan, T Tjahjowidodo, Use of Acoustic Emissions to detect change in contact mechanisms caused by tool wear in abrasive belt grinding process. *Wear*, 2019, 436: 203047.
- [8] T T Wang, L Zou, Q H Wan, et al. A high-precision prediction model of surface roughness in abrasive belt flexible grinding of aero-engine blade. *Journal of Manufacturing Processes*, 2021, 66: 364-375.
- [9] W X Wang, F Salvatore, J Rech. Characteristic assessment and analysis of residual stresses generated by dry belt finishing on hard turned AISI52100. *Journal of Manufacturing Processes*, 2020, 59: 11-18.
- [10] W Wang, C Yun. A path planning method for robotic belt surface grinding. *Chinese Journal of Aeronautics*, 2011, 24(4): 520-526.
- [11] C Lv, L Zou, Y Huang, et al. A trajectory planning method on error compensation of residual height for aero-engine blades of robotic belt grinding. *Chinese Journal of Aeronautics*, 2022, 35(4): 508-520.
- [12] Z X Wang, T Q Zhang, T B Yu, et al. Assessment and optimization of grinding process on aisi 1045 steel in terms of green manufacturing using orthogonal experimental design and grey relational analysis. *Journal of Cleaner Production*, 2020, 253: 119896.
- [13] Z H Deng, H Zhang, Y H Fu, et al. Optimization of process parameters for minimum energy consumption based on cutting specific energy consumption. *Journal of Cleaner Production*, 2017, 166: 1407-1414.
- [14] T Kizaki, K Takahashi, T Katsuma, et al. Prospects of dry continuous generating grinding based on specific energy requirement. *Journal of Manufacturing Processes*, 2021, 61: 190-207.
- [15] H N Li, D Axinte, On a stochastically grain-discretised model for 2d/3d temperature mapping prediction in grinding. *International Journal of Machine Tools and Manufacture*, 2017, 116: 60-76.
- [16] M Kadivar, B Azarhoushang, U Klement, et al. The role of specific energy in micro-grinding of titanium alloy. *Precision Engineering*, 2021, 72: 172-183.
- [17] S Malkin, T W Hwang. Grinding mechanisms for ceramics. *CIRP Annals*, 1996, 45: 569-580.
- [18] A Khellouki, J Rech, H Zahouani. Energetic analysis of cutting mechanisms in belt finishing of hard materials. *Part B: Journal of Engineering Manufacture*, 2013, 227: 1409-1413.
- [19] D H Zhu, S Y Luo, L Yang, et al. On energetic assessment of cutting mechanisms in robot-assisted belt grinding of titanium alloys. *Tribology International*, 2015, 90: 55-59.
- [20] D H Zhu, X H Xu, Z Y Yang, et al. Analysis and assessment of robotic belt grinding mechanisms by force modeling and force control experiments. *Tribology International*, 2018, 120: 93-98.
- [21] Z He, J Y Li, Y M Liu, et al. Investigation on wear modes and mechanisms of abrasive belts in grinding of U71Mn steel. *The International Journal of Advanced Manufacturing Technology*, 2019, 101(5-8): 1821-1835.
- [22] K Wegener, H W Hoffmeister, B Karpuschewski, et al. Conditioning and monitoring of grinding wheels. *CIRP Annals*, 2011, 60 (2): 757-777.
- [23] L F Li, X K Ren, H J Feng, et al. A novel material removal rate model based on single grain force for robotic belt grinding. *Journal of Manufacturing Processes*, 2021, 68: 1-12.
- [24] X Q Zhang, H B Chen, J J Xu, et al. A novel sound-based belt condition monitoring method for robotic grinding using optimally pruned extreme learning machine. *Journal of Materials Processing Technology*, 2018, 260: 9-19.
- [25] Y Huang, Y Wu, G J Xiao, et al. Analysis of abrasive belt wear effect on residual stress distribution on a grinding surface. *Wear*, 2021, 486: 204113.
- [26] G Y Luo, L Zou, Z L Wang, et al. A novel kinematic parameters calibration method for industrial robot based on levenberg-marquardt and differential evolution hybrid algorithm. *Robotics and Computer-Integrated Manufacturing*, 2021, 71: 102165.
- [27] Z L Wang, L Zou, L Duan, et al. Study on passive compliance control in robotic belt grinding of nickel-based superalloy blade. *Journal of Manufacturing Processes*, 2021, 68: 168-179.

- [28] M Li, B H Lyu, J L Yuan, et al. Evolution and equivalent control law of surface roughness in shear-thickening polishing. *International Journal of Machine Tools and Manufacture*, 2016, 108: 113-126.
- [29] T K Puthanangady, S Malkin. Experimental investigation of the superfinishing process. *Wear*, 1995, 185(1-2): 173-182.
- [30] X K Ren, X K Huang, Z Chai, et al. A study of dynamic energy partition in belt grinding based on grinding effects and temperature dependent mechanical properties. *Journal of Materials Processing Technology*, 2021, 294: 1171-112.
- [31] S Mezghani, M El Mansori. Abrasiveness properties assessment of coated abrasives for precision belt grinding. *Surface and Coatings Technology*, 2008, 203(5-7): 786-789.
- [32] J Schmähling, F A Hamprecht. Generalizing the Abbott–Firestone curve by two new surface descriptors. *Wear*, 2007, 262(11-12): 1360-1371.
- [33] Y Z Pu, Y G Zhao, H Y Zhang, et al. Study on the three-dimensional topography of the machined surface in laser-assisted machining of Si_3N_4 ceramics under different material removal modes. *Ceramics International*, 2020, 46(5): 5695-5705.

Submit your manuscript to a SpringerOpen[®] journal and benefit from:

- ▶ Convenient online submission
- ▶ Rigorous peer review
- ▶ Open access: articles freely available online
- ▶ High visibility within the field
- ▶ Retaining the copyright to your article

Submit your next manuscript at ▶ [springeropen.com](https://www.springeropen.com)
